Inorg. Chem. **2004**, *43*, 132−141

Transient Mixed-Valence Character of $Re^{I}_4(CO)_{12}(4,4'\text{-bpy})_4Cl_4$

Theodore P. Ortiz, Jason A. Marshall, Luke A. Emmert, Jing Yang, Wonsook Choi, Alison L. Costello, and James A. Brozik*

Department of Chemistry, The University of New Mexico, Albuquerque, New Mexico 87131

Received May 23, 2003

This study addresses, in detail, the orbital nature and the extent of metal–metal communication in the lowest emitting triplet state of $Re_4(CO)_{12}(4,4'\text{-bpy})_4Cl_4$ (where 4,4′-bpy = 4,4′-bipyridine) as well as the symmetry of the lowest ^{3}MLCT manifold in comparison to that of the ground state. All spectral evidence points to (1) a ^{3}MLCT excited manifold localized between a single Re(I) corner and an adjacent bridging ligand, (2) a transient mixed-valence state that is completely localized between a single transiently oxidized Re center and the adjacent metals, and (3) a second-order charge transfer from a localized transiently reduced bridging ligand to the adjacent Re(I) center to which it is attached, effectively lowering its oxidation state. The orbital nature of the lowest ^{3}MLCT manifold is fully corroborated by a molecular orbital diagram derived from quantum chemical modeling studies, while the existence of the localization, localized mixed valency, and second-order charge transfer rely on spectral evidence alone. This work makes use of low-temperature time-resolved infrared (TRIR) techniques as well as a luminescence study. Many of the nuances of the luminescence and TRIR data interpretation are extracted from statistical analysis and quantum chemical modeling studies. The relative concentrations of the dominant conformers that exist for $Re_4(CO)_{12}(4,4'\text{-bpy})_4Cl_4$ have also been estimated from Boltzmann statistics.

I. Introduction

Self-assembled coordinately bound nanometer-sized molecules and network polymers containing transition metals have long intrigued scientists in many different fields ranging from chemistry to condensed matter physics.[1−4] Such materials combine the enormous electronic tunability, rich photophysical characteristics, and photochemical properties of transition-metal complexes with variable size, intrinsic cavities, and unique electronic coupling patterns that are entirely different from their pure inorganic or organic counterparts.[5,6] These intrinsic physical and structural properties make these materials ideal for potential use in device applications, solar energy conversion, and photocatalysis.[7,8] Of particular interest in the current study are tetrametallic coordination compounds that possess a square structural motif. This class of molecules has received much attention in the past few years, mostly because their nanometer-sized interior cavities (0.5−3.0 nm) have been shown to be useful in selective guest−host chemistry, size-selective transport, chemical sensing, and chemical catalysis to name but a few pertinent applications.[7−18]

In terms of spectroscopic properties, the exact orbital assignments of the excited states associated with multimetallic coordination compounds present a very interesting

* Author to whom correspondence should be addressed. E-mail: brozik@unm.edu.

(1) Moulton, B.; Zaworotko, M. J. *Chem. Rev.* **2001**, *101*, 1629−1658.
(2) Bignozzi, C. A.; Argazzi, R.; Kleverlaan, C. J. *Chem. Soc. Rev.* **2000**, *29*, 87−96.
(3) Piguet, C.; Bernardinelli, G.; Hopfgartner, G. *Chem. Rev.* **1997**, *97*, 2005−2062.
(4) Swiegers, G. F.; Malefetse, T. *Chem. Rev.* **2000**, *100*, 3483−3537.
(5) Balzani, V.; Alberto, C.; Margherita, V. *Coord. Chem. Rev.* **1998**, *171*, 3−16.
(6) Le Bozec, H. L.; Le Bouder, T. L.; Maury, O.; Ledoux, I.; Zyss, J. *J. Opt. A: Pure Appl. Opt.* **2002**, *4*, S189−S196.
(7) Keefe, M. H.; Benkstein, K. D.; Hupp, J. T. *Coord. Chem. Rev.* **2000**, *205*, 201−228.
(8) Dinolfo, P. H.; Hupp, J. T. *Chem. Mater.* **2001**, *13*, 3113−3125.
(9) Williams, M. E.; Benkstein, K. D.; Abel, C.; Dinolfo, P. H.; Hupp, J. T. *Proc. Natl. Acad. Sci. U.S.A.* **2002**, *99*, 5171−5177.
(10) Nquyen, S. T.; Gin, D. L.; Hupp, J. T.; Zhang, X. *Proc. Nat. Acad. Sci. U.S.A.* **2001**, *98*, 11849−11850.
(11) Williams, M. E.; Hupp, J. T. *J. Phys. Chem.* **2001**, *105*, 8944−8950.
(12) Keefe, M. H.; Slone, R. V.; Hupp, J. T.; Czaplewski, K. F.; Snurr, R. Q.; Stern, C. L. *Langmuir* **2000**, *16*, 3964−3970.
(13) Belanger, S.; Hupp, J. T.; Stern, C. L.; Slone, R. V.; Watson, D. F.; Carrell, T. G. *J. Am. Chem. Soc.* **1999**, *121*, 557−563.
(14) Benkstein, K. D.; Hupp, J. T.; Stern, C. L. *Angew. Chem., Int. Ed. Engl.* **2000**, *39*, 2891−2893.
(15) Slone, R. V.; Yoon, D. I.; Calhoun, R. M.; Hupp, J. T. *J. Am. Chem. Soc.* **1995**, *117*, 11813−11814.
(16) Slone, R. V.; Hupp, J. T. *Inorg. Chem.* **1997**, *36*, 5422−5423.
(17) Benkstein, K. D.; Hupp, J. T.; Stern, C. L. *J. Am. Chem. Soc.* **1998**, *120*, 12982−12983.
(18) Lees, A. J.; Sun, S. S. *J. Am. Chem. Soc.* **2000**, *122*, 8956−8967.

10.1021/ic034560l CCC: $27.50
Published on Web 12/03/2003

challenge in that a number of excited states can, and often do, lie in very close proximity to one another, leading to complicated luminescence properties and ambiguous state assignments. Moreover, the highly symmetrical nature of square coordination compounds can lead to important, and often missed, second-order charge-transfer effects as electron density is redistributed in the excited states. Because of the rather complicated electronic nature of the excited states in this class of molecules, it is advantageous to apply other spectroscopic tools, in addition to time-resolved luminescence spectroscopy, to aid in definitive state assignments. Time-resolved infrared (TRIR) spectroscopy was used in the current study for this purpose.

Beyond the orbital specification of the lowest emitting excited state(s), the more intriguing question of excited-state localization (or delocalization) in multimetallic transition-metal complexes, and the consequences resulting from the transient mixed valency between adjacent metal atoms, is of particular interest, because the physical and chemical properties can vary so widely with simple chemical substitution.[19] Two particularly interesting examples that are directly related to the present work are the separate TRIR studies of the bimetallic rhenium complex $[(dmb)(CO)_3Re^{I}(4,4'\text{-bpy})\text{-}Re^{I}(CO)_3(dmb)]$ (where dmb = 4,4′-dimethyl-2,2′-bipyridine) by Meyer et al. and the bimetallic tungsten complexes $[(CO)_5W(L)W(CO)_5]$ (where L = 4,4′-bipyridine or pyrazine) by Turner et al.[20−22] In these studies, it has been shown that the lowest excited triplet is a ^{3}MLCT that localizes an electron on the bridging ligand. The consequence of such localized charge transfer is that the molecule becomes effectively mixed-valent in the excited state, and the question of whether the transient oxidation is localized on a single metal or delocalized naturally arises. In both cases it was shown that the transient mixed-valence character is completely localized, viz., $[Re^{2+}-Re^{1+}]^*$ and $[W^{+}-W^{0}]^*$.

A similar set of questions naturally arises when the excited states of the square transition-metal complex $Re_4(CO)_{12}(4,4'\text{-bpy})_4Cl_4$ are studied, although the analysis does become more complicated. In the present case there are four nearly equivalent bridging ligands, making localization of the promoted electron not a forgone conclusion. In addition, if the promoted electron does localize on one of the bridging ligands, then the transient mixed-valence excited state is present not only between the metals directly attached to the transiently reduced ligand, but also between metals bridged by the nonreduced ligand. In this paper we address these issues using TRIR and luminescence spectroscopies at low temperatures, as well as quantum chemical modeling.

II. Experimental Section

(A) Synthesis and Materials. $Re_4(CO)_{12}(4,4'\text{-bpy})_4Cl_4$ was synthesized from literature methods.[13,23] Afterward, it was further purified using a silica gel column with reagent-grade acetone as the eluent and recrystallized by slow evaporation of the solvent. X-ray crystallography confirmed the crystallization of a single isomer with a puckered conformation as observed by Hupp et al. (Note: this is not to say that other isomers were not formed during the synthesis, only that a single isomer was isolated by recrystallization from acetone.) $Re(CO)_5Cl$ was purchased from Aldrich Chemical Co. and used as received. 4,4′-Bipyridine was also purchased from Aldrich and sublimed prior to use. All solvents were reagent grade and freshly distilled. The IR (acetone) spectrum, ^{1}H NMR (acetone-d_6) spectrum, and luminescence properties were all identical to those reported in the literature.[13,23]

(B) Sample Preparation for Spectroscopic Studies. All solvents were reagent grade (purchased from EM Science) and freshly distilled and degassed prior to use. Poly(methyl methacrylate) (PMMA), having a molecular weight of ∼120000, was purchased from Aldrich and was used as received. All samples for spectroscopic study were prepared as thin films of PMMA. This was achieved by dissolving ∼1 mg of sample and 100 mg of PMMA in acetone, from which a plastic film was made. For 77 K steady-state emission, luminescence lifetime, and TRIR experiments, thin films of PMMA were prepared by casting the solution in shallow aluminum molds and allowing them to dry (∼24 h) under an argon atmosphere. The resultant thin films, which were peeled from their aluminum molds after drying, had an average thickness of ∼90 μm. The exact concentration of sample in PMMA was adjusted so that the thin films had an average maximum IR absorbance of ∼0.3 at 2025 cm^{-1} and 77 K. PMMA plastics have a clear IR window from 2828 to 1760 cm^{-1}. While the above-mentioned method for producing thin films was appropriate for luminescence and TRIR experiments, it was not suitable for ground-state FTIR experiments, in which the samples and reference backgrounds needed to be the same thickness. Therefore, PMMA samples and PMMA blanks were prepared on CaF_2 optical flats using a spin coater (Headway Inc. model 1-EC101D-R790). During the spin-coating process, the samples were exposed to air. Since these films were much thinner than the delaminated films described above, the optical absorbance in the carbonyl region was considerably smaller.

(C) Steady-State Emission. Steady-state emission spectra were obtained from samples mounted onto a custom-made sample holder, immersed directly into a bath of liquid nitrogen inside a quartz optical dewar. The excitation source was a 150 W Xe arc lamp that had been filtered with a combination of a $CuSO_4$ water filter and a UV band-pass filter to isolate a broad UV band peaking at 360 nm and focused directly onto the sample with a spherical quartz lens. The emitted light was monitored at 90° to the excitation beam, filtered through a 33 M KNO_2 filter (to remove the exciting UV), dispersed by an Acton 500i monochromator, and detected by a thermoelectrically cooled Hamamatsu R943-02 photomultiplier. The detector signal was passed through a wide-band preamplifier and fed to a Stanford Research Systems SR400 photon counter. Data were transferred to a PC for further manipulation. All spectra were corrected against a quartz−tungsten−halogen spectral irradiance standard lamp (Oriel Inc.).

(D) Luminescence Lifetimes. For luminescence decay-time measurements at 77 K, the sample preparation method and detection system were as described above. The excitation source was the tripled output of a Nd:YAG laser (Continuum Minilite, 355 nm, 4 ns pulse width, 1 μJ pulse energy). An optical trigger synchronized the photon counter to the pulse train. The data were transferred to

(19) Demadis, K. D.; Hartshorn, C. M.; Meyer, T. J. *Chem. Rev.* **2001**, *101*, 2655−2685.
(20) Omberg, K. M.; Schoonover, J. R.; Meyer, T. J. *J. Phys. Chem. A* **1997**, *101*, 9531−9536.
(21) George, M. W.; Turner, J. J.; Westwell, J. R. *J. Chem. Soc., Dalton Trans.* **1994**, 2217−2219.
(22) George, M. W.; Johnson, F. P. A.; Turner, J. J.; Westwell, J. R. *J. Chem. Soc., Dalton Trans.* **1995**, 2711−2718.
(23) Slone, R. V.; Hupp, J. T.; Stern, C. L.; Albrecht-Schmitt, T. E. *Inorg. Chem.* **1996**, *35*, 4096−4097.

a PC for further analysis. All data reduction was achieved by means of a curve-fitting program (IGOR, Wavemetrics Inc.).

(E) Low-Temperature FTIR. FTIR spectra were measured with a Nicolet Nexus 870 FTIR spectrophotometer. Samples were spread across a 3 mm hole drilled into a custom-made bronze sample holder that was subsequently attached to the thermal base of a 77 K cryostat (Janis Inc. model VPF-100). The cryostat was equipped with CaF_2 windows for both UV−vis and IR experiments. The temperature was monitored with a calibrated silicon cryodiode (Lake Shore Cryotronics Inc. model DT-470-SC-13-1.4L) and controlled with a temperature controller (Lake Shore Cryotronics Inc. model 330). The cryostat was mounted directly into the sample compartment of the spectrophotometer via a custom-made mounting plate and aligned with a mechanical stage. All spectra were recorded at 8 cm^{-1} resolution with a liquid nitrogen cooled MCT detector.

(F) Time-Resolved IR Spectroscopy at 77 K. In this experiment, samples were mounted and cooled to 77 K in the Janis cryostat as described above. The entire TRIR spectroscopic experiment was sealed around the cryostat and purged with a continual stream of dry N_2. Electronic excitation was achieved by the tripled output of a Nd:YAG laser (Continuum Minilite, 355 nm, 4 ns pulse width, 50 μJ pulse energies), and transient IR signatures were probed with a commercial step-scan FTIR (SS-FTIR) spectrometer (Nicolet Nexus 870). The laser power was chosen to eliminate photoinduced decomposition. Care was taken to overlap the excitation pulse with the IR probe (3 mm diameter). The spectral range of the IR probe was limited by a long-pass filter (Janos F1305L300) and the CaF_2 windows of the Janis cryostat (spectral range 3200−1111 cm^{-1}). Timing between the interferometer and the laser was achieved with an optical trigger (photodiode, ThorLabs model DET210), and the entire time domain was recorded with a 100 MHz digital oscilloscope (Gage model 12100-1M). In the SS-FTIR spectroscopic study the moveable mirror of the interferometer was moved stepwise in 1.264 μm increments. The mirror was then held stationary at each fixed position while the data were collected. Two sets of data were acquired after each mirror step: one from the ac-coupled output of the MCT detector and the other from its dc-coupled output. The dc signal was collected before the laser was fired and, after a Fourier transform, constituted the single-beam static background spectrum. The ac signal was synchronized to the pulse train of the laser and, after a Fourier transform of each time slice, constituted the dynamic time-resolved IR spectral profile recorded at several time delays (30) after each laser pulse. The static spectrum was collected as a time average (250 ms) at each mirror position, while the dynamic spectra were collected as a numerical average of 150 laser pulses at each mirror position. The dynamic interferogram at each time delay was obtained by the manipulation of the full array of kinetic data versus mirror position (volts vs mirror position vs time). All time-resolved spectra are plotted as the change in absorbance (ΔA), which is calculated as $\Delta A = \log(1 + \text{dynamic/static})$ (where "dynamic" = dynamic single-beam spectrum and "static" = static single-beam spectrum).[24] All spectra reported are the average of five individual experiments.

(G) Electronic and Frequency Calculations. All quantum mechanical modeling studies employed Gaussian 98W software (version 5.2, revision A.7) which was implemented on a PC running the Microsoft Windows 98 operating system.[25] Molecular orbital diagrams were determined using optimized geometries. MO diagrams and ground-state vibrational frequencies (IR spectra) were generated using Hartree−Fock (HF) and density functional theory (DFT). Two different basis sets were used to build the MO diagrams; these included standard Gaussian basis sets (ST0-3G and 3-21G) on all elements except the transition metals, for which the Stuttgart−Dresden relativistic small core potential (SDD) or the LANL2DZ ECP was used.[26] All frequencies were calculated utilizing the 3-21G basis set and then corrected with published frequency correction factors.[27−29]

There are four possible isomers for $Re_4(CO)_{12}(4,4'\text{-bpy})_4Cl_4$: one in which all the axial Cl^- ligands are on the same side, one in which the axial Cl^- ligands alternate (see Figure 1), one in which two adjacent axial Cl^- ligands point in the same direction, and finally one in which three of the axial Cl^- ligands point in the same direction while the fourth points in the opposite direction. There is no doubt that all four isomers are formed during synthesis, but the isomer in which the axial ligands alternate can be isolated from the others by recrystallization from acetone. Since it is this isomer that we have isolated and spectroscopically investigated, we have also limited our modeling to that isomer. This structural isomer can give rise to two conformational isomers: one in which the square is severely puckered out of plane and the other having a more planar geometry (see Figure 1). This is in accordance with the experimental results reported by Hupp and co-workers (see refs 7 and 16 for X-ray structures). It should also be noted that the two X-ray structures were published separately and the more planar configuration did display disorder among the axial ligands while the puckered configuration did not.[13,23] The disordered structure observed for the planar configuration is most probably due to the existence of more than one isomer. The puckered configuration is observed for the single isomer with alternating axial ligands isolated from a recrystallization step from acetone. To find the minimum SCF (self-consistent field) geometries for the planar and puckered conformers, we utilized published X-ray data as our starting points. Because the experimentally observed planar structure displays disorder in the axial ligands, the procedure for obtaining an SCF minimized geometry for the planar conformers was to start with the experimental data and substitute average bond lengths and ideal bond angles for the axial ligands, after which a geometry optimization was performed.[23] Because of the relative orientations of the pyridine rings in the X-ray data, there were two possible ways to place the alternating axial ligands; however, both starting points lead to a single SCF minimum within the planar motif. The X-ray

(24) Chen, P.; Palmer, R. A. *Appl. Spectrosc.* **1997**, *51*, 580−583.

(25) Frisch, M. J.; Trucks, G. W.; Schlegel, H. B.; Scuseria, G. E.; Robb, M. A.; Cheeseman, J. R.; Zakrzewski, V. G.; Montgomery, J. A., Jr.; Stratmann, R. E.; Burant, J. C.; Dapprich, S.; Millam, J. M.; Daniels, A. D.; Kudin, K. N.; Strain, M. C.; Farkas, O.; Tomasi, J.; Barone, V.; Cossi, M.; Cammi, R.; Mennucci, B.; Pomelli, C.; Adamo, C.; Clifford, S.; Ochterski, J.; Petersson, G. A.; Ayala, P. Y.; Cui, Q.; Morokuma, K.; Salvador, P.; Dannenberg, J. J.; Malick, D. K.; Rabuck, A. D.; Raghavachari, K.; Foresman, J. B.; Cioslowski, J.; Ortiz, J. V.; Baboul, A. G.; Stefanov, B. B.; Liu, G.; Liashenko, A.; Piskorz, P.; Komaromi, I.; Gomperts, R.; Martin, R. L.; Fox, D. J.; Keith, T.; Al-Laham, M. A.; Peng, C. Y.; Nanayakkara, A.; Challacombe, M.; Gill, P. M. W.; Johnson, B.; Chen, W.; Wong, M. W.; Andres, J. L.; Gonzalez, C.; Head-Gordon, M.; Replogle, E. S.; Pople, J. A.; *Gaussian 98W*, A.7 ed.; Gaussian: Pittsburgh, PA, 2001.

(26) Basis sets were obtained from the Extensible Computational Chemistry Environment Basis Set Database, version 2/12/03, as developed and distributed by the Molecular Science Computing Facility, Environmental and Molecular Sciences Laboratory, which is part of the Pacific Northwest Laboratory, P.O. Box 999, Richland, WA 99352, and is funded by the U.S. Department of Energy. The Pacific Northwest Laboratory is a multiprogram laboratory operated by Battelle Memorial Institute for the U.S. Department of Energy under Contract DE-AC06-76RLO 1830. Contact David Feller or Karen Schuchardt for further information.

(27) Pople, J. A.; Scott, A. P.; Wong, M. W.; Radom, L. *Isr. J. Chem.* **1993**, *33*, 345−350.

(28) Scott, A. P.; Radom, L. *J. Phys. Chem.* **1996**, *100*, 16502−16513.

(29) Wong, M. W. *Chem. Phys. Lett.* **1996**, *256*, 391−399.

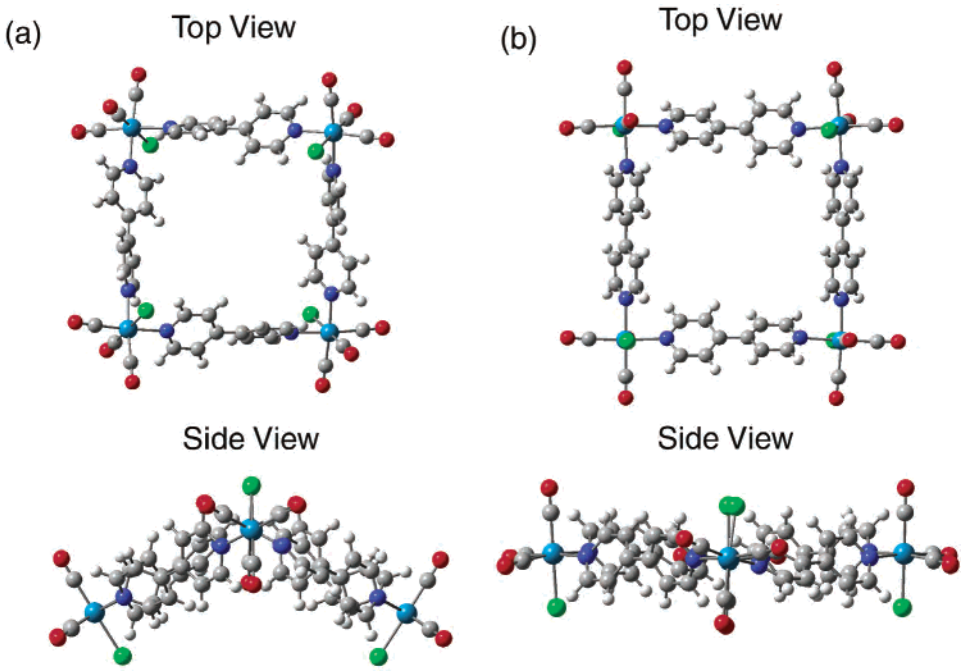

Figure 1. SCF-geometry-optimized molecular structures of $Re_4(CO)_{12}(4,4'\text{-bpy})_4Cl_4$. Shown are the results of two separate HF/STO-3G/SDD calculations: (a) puckered geometry, (b) planar geometry.

data for the puckered motif have also revealed two similar puckered geometries that converged to a single SCF minimum within the puckered motif. For completeness we modeled both experimentally observed conformational isomers, and their geometries are depicted in Figure 1. Moreover, attempts were made to find additional planar and puckered conformers by rotating the pyridine rings of the bridging ligands relative to one another before geometry optimizations were performed.

III. Results

(A) Emission Spectra. $Re_4(CO)_{12}(4,4'\text{-bpy})_4Cl_4$ is highly luminescent from 4.2 K to room temperature in a variety of matrices, such as PMMA plastics, organic glasses, and fluid solutions, and also in the solid state (crystals). We have observed that while related compounds, such as $Re(CO)_3(2,2'\text{-bpy})Cl$, are relatively photochemically robust in most fluid solutions, $Re_4(CO)_{12}(4,4'\text{-bpy})_4Cl_4$ is much more susceptible to photochemical decomposition in solvents such as CH_2Cl_2, acetone, and CH_3CN. Because of this, all of the spectroscopic experiments have been conducted in clear PMMA plastic films at 77 K with excitation powers that yielded no detectable decomposition. Shown in Figure 2 is the normalized 77 K luminescence spectrum of $Re_4(CO)_{12}(4,4'\text{-bpy})_4Cl_4$ in a PMMA plastic film.

This spectrum consists of a single, broad, structureless, and long-lived luminescence band that has been assigned to a ^{3}MLCT $\rightarrow$ ^{1}ground-state (^{1}GS) phosphorescence. This is in accordance with the assignments made by a number of researchers that have reported the room-temperature luminescence spectrum of $Re_4(CO)_{12}(4,4'\text{-bpy})_4Cl_4$, as well as the luminescence assignments made for related compounds, including a number of Re(I) squares.[18,23,30−36] The orbital character of the phosphorescent ^{3}MLCT manifold arises from a $5d_{Re} \rightarrow \pi^*_{4,4'-bpy}$ HOMO-to-LUMO promotion. This orbital

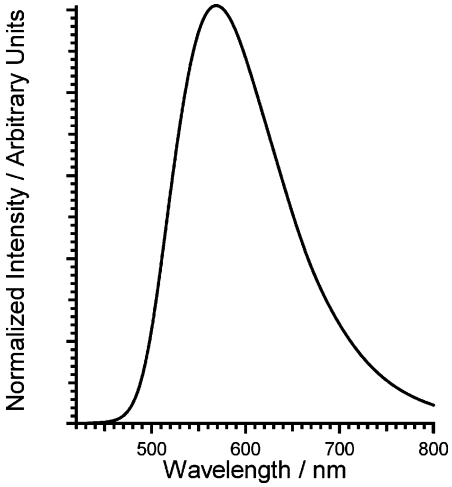

Figure 2. Steady-state luminescence spectrum of $Re_4(CO)_{12}(4,4'\text{-bpy})Cl_4$ at 77 K in PMMA. The sample was excited with a broad UV band peaking at 360 nm.

assignment is corroborated by TRIR spectroscopic evidence and detailed quantum chemical modeling studies (vide infra). It should be noted that the emission from the triplet manifold arises from three low-lying Boltzmann-populated states that have been split by spin−orbit coupling.[34,37]

(30) Slone, R. V.; Benkstein, K. D.; Belanger, S.; Hupp, J. T.; Guzei, I. A.; Rheingold, A. L. *Coord. Chem. Rev.* **1998**, *171*, 221−243.
(31) Slone, R. V.; Yoon, D. I.; Calhoun, R. M.; Hupp, J. T. *J. Am. Chem. Soc.* **1995**, *117*, 11813−11814.
(32) Woessner, S. M.; Helms, J. B.; Houlis, J. F.; Sullivan, B. P. *Inorg. Chem.* **1999**, *38*, 4380−4381.
(33) Woessner, S. M.; Helms, J. B.; Lantzky, K. M.; Sullivan, B. P. *Inorg. Chem.* **1999**, *38*, 4378−4379.
(34) Striplin, D. R.; Crosby, G. A. *Chem. Phys. Lett.* **1994**, *221*, 429−430.
(35) Striplin, D. R.; Crosby, G. A. *Coord. Chem. Rev.* **2001**, *211*, 163−175.
(36) Tapolsky, G.; Duesing, R.; Meyer, T. J. *J. Phys. Chem.* **1991**, *95*, 1105−1112.

Table 1. Luminescence Lifetimes[a,b]

molecule	τ_{lum} (μs)	τ_{TRIR} (μs)
$Re_4(CO)_{12}(4,4\text{-bpy})_4Cl_4$	18.8 ± 0.1	18.9 ± 0.5

[a] The luminescence lifetime was measured at 77 K with the tripled output of a Nd:YAG laser attenuated to produce a 1 μJ pulse and focused to a 3 mm spot size. [b] The TRIR lifetime was measured at 77 K with the tripled output of a Nd:YAG laser focused to a 3 mm spot size with the pulse energy attenuated to 50 μJ.

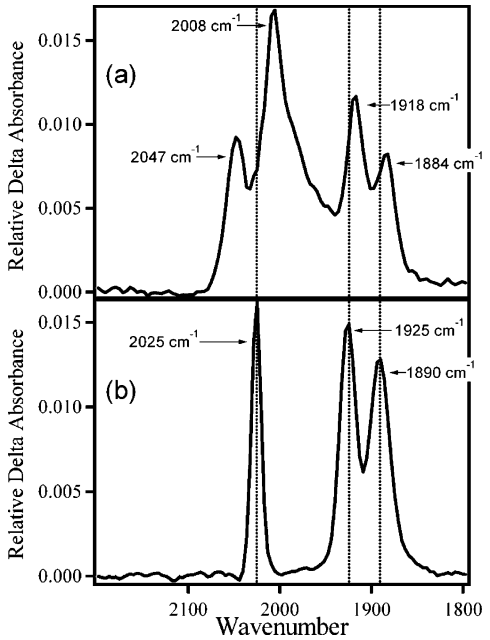

Figure 3. $Re_4(CO)_{12}(4,4'\text{-bpy})_4Cl_4$ in PMMA at 77 K: (a) excited-state IR spectrum, first 2 μs time slice, 355 nm laser excitation, 50 μJ laser pulse, 4 ns pulse width (note: the relative ΔA is defined as the original ground-state FTIR spectrum scaled to the amount added back into the TRIR data to produce the excited-state IR spectrum), (b) ground-state FTIR spectrum.

(B) Lifetimes. The phosphorescence lifetime for $Re_4(CO)_{12}(4,4'\text{-bpy})_4Cl_4$ embedded in PMMA plastic films and measured at 77 K is listed in Table 1. The luminescence decay curve was fit to a single exponential over five lifetimes. The time scale of the luminescence lifetime confirms the phosphorescent nature of the luminescence band, and the single-exponential behavior indicates that $Re_4(CO)_{12}(4,4'\text{-bpy})_4Cl_4$ is emitting from a single Boltzmann-populated excited triplet manifold.

(C) Infrared Spectra. The ground-state IR spectrum in the CO stretching region of $Re_4(CO)_{12}(4,4'\text{-bpy})_4Cl_4$ in PMMA at 77 K is depicted in Figure 3b. It should be noted that the 77 K PMMA spectrum is nearly identical to those measured at room temperature in solutions of acetone and dichloromethane (i.e., no detectable ground-state rigidochromism). The IR spectrum displays three distinct carbonyl stretches at 2025, 1925, and 1890 cm^{-1}, corresponding to three distinct normal modes formed from the carbonyls around each individual Re center. The normal mode assignment for the ground state is schematically depicted in Figure 4. These normal mode assignments are based on quantum chemical frequency calculations as described above and

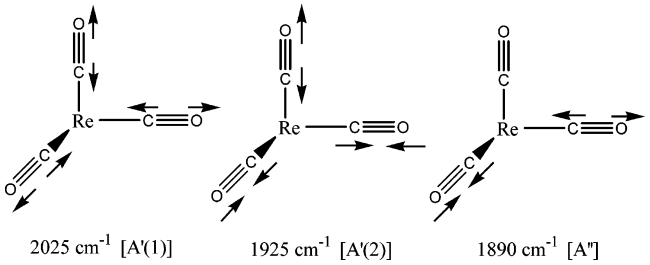

Figure 4. Infrared assignments for carbonyl normal modes of vibration around each individual Re(I) center. The symmetry labels are included for quick literature comparison with related Re(I) compounds and are based on the C_{3v} point group (the approximate site symmetry of the CO ligands around the Re metals).

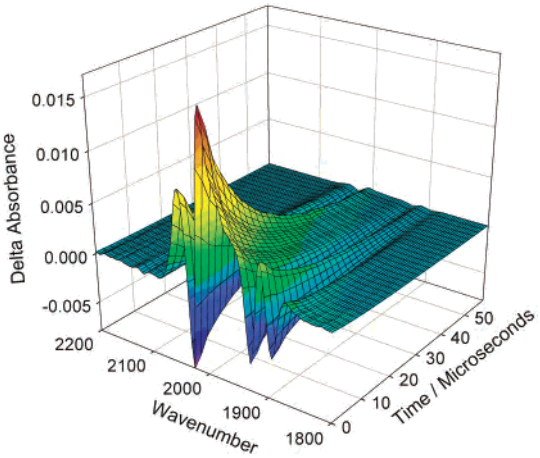

Figure 5. TRIR spectrum of $Re_4(CO)_{12}(4,4'\text{-bpy})Cl_4$ in PMMA plastic at 77 K. Laser excitation is 355 nm, with 50 μJ/pulse, a 10 Hz repetition rate, and a 4 ns pulse width. Each time slice is 2 μs. The entire data set was "smoothed" with an SVD analysis.

previous normal mode assignments for $Re(CO)_3(2,2'\text{-bpy})Cl$ and related molecules.[38]

(D) Excited-State Infrared Signatures. The dynamic TRIR data were collected through the ac-coupled output of the MCT detector. Because of this, the ac spectrum only records IR signatures that change in response to the applied laser excitation, which is, in turn, synchronized to the digital storage oscilloscope. Static IR absorptions are silent. Therefore, the TRIR data can be interpreted in terms of a change in optical density vs time. The TRIR data (after a Fourier transform and conversion to ΔA) are displayed in Figure 5, and the excited-state IR spectrum (in relative ΔA) is displayed in Figure 3a. Since the TRIR data contain both the grow-in of the excited-state IR spectrum and the bleach of the ground-state IR spectrum, the excited-state IR spectrum was derived from the initial 2 μs time slice of the TRIR data and the ground-state IR spectrum. The latter was simply added back into the TRIR data (i.e., subtracting out the ground-state bleach).

In the carbonyl region, the excited-state IR spectrum of $Re_4(CO)_{12}(4,4'\text{-bpy})_4Cl_4$ displays four well-resolved peaks superimposed on top of a less resolved transient signature. These are at 2047, 2008, 1918, and 1884 cm^{-1}.

(37) Crosby, G. A. *Acc. Chem. Res.* **1975**, *8*, 231−238.

(38) Dattelbaum, D. M.; Omberg, K. M.; Schoonover, J. R.; Martin, R. L.; Meyer, T. J. *Inorg. Chem.* **2002**, *41*, 6071−6079.

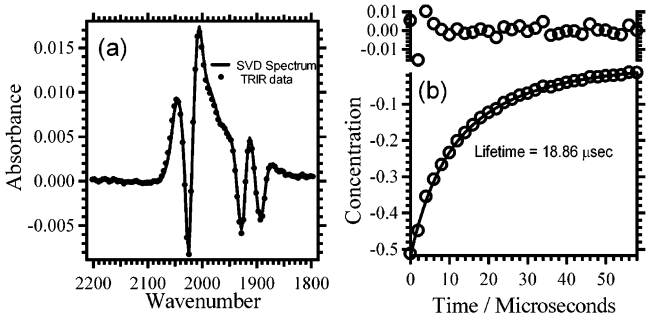

Figure 6. Results of SVD analysis: (a) (●) raw TRIR data from PMMA plastic; (—) eigenvector extracted from SVD analysis; (b) (○) propagation vector from SVD analysis; (—) exponential fit.

To explore the time evolution of the TRIR spectra, the data have been analyzed with the technique of singular value decomposition (SVD).[39−42] This global analysis was used to determine the number of temporally distinct IR signatures that exist in the time-resolved data (basis spectra), as well as their relative weights (eigenvalues), and to extract the time dependence of each of the corresponding eigenvectors (propagation vectors). If, for example, the observed TRIR spectra arise from the composition of three distinct excited states exhibiting three distinct time evolutions, then the SVD analysis can, in principle, completely separate these out. One can also use SVD to extract the eigenvectors from random noise. The analysis works by expressing the entire time-dependent data set in terms of

$$\Delta A(\mathrm{cm}^{-1},t) = \bar{U}\bar{S}\bar{T}'$$

where $\bar{U}$ is an $m \times n$ matrix whose columns are comprised of all nonzero eigenvectors (or basis spectra) that make up the original data set. $\bar{S}$ is an $n \times n$ diagonal matrix of eigenvalues (positive and decreasing) which will properly weight each eigenvector, and $\bar{T}$ is an $n \times n$ matrix describing the composition of the original matrix in terms of the basis spectra (i.e., each column of $\bar{T}$ describes the time propagation of each basis spectrum). SVD analysis is built into a number of mathematical software packages; MATLAB 6.5 was used in the present study.

The results of the SVD analysis are shown in Figure 6. This present case reveals a trivial solution in which only a single TRIR spectrum is found, and that spectrum decays with a single-exponential lifetime. One can see that the calculated eigenvector nicely reproduces the experimental TRIR spectrum and that the time dependence is fit by a single exponential that is commensurate with the experimentally measured luminescence lifetime (see Table 1). This is conclusive evidence that the TRIR experiment is indeed probing the same excited state as that probed by the luminescence experiments (i.e., the lowest vibrationally relaxed ^{3}MLCT manifold) in accordance with the Crosby−Kasha rule.[43]

(E) $Re_4(CO)_{12}(4,4'\text{-bpy})_4Cl_4$ MO Diagram. Experimentally it has been shown that $Re_4(CO)_{12}(4,4'\text{-bpy})_4Cl_4$ can be crystallized as either a puckered or a planar conformer[13,23] as shown in Figure 1. When presented with such a result, two questions come to mind: First, which conformer is lowest in energy? Second, what are the relative concentrations of each under normal experimental conditions? We have addressed both of these questions by employing the HF-SCF method to determine the energy difference between each conformer in their ground states. Using HF/STO-3G/SDD, two local minima associated with the two different conformational isomers were found by starting with the experimentally observed structures and then performing separate geometry optimizations. We have also "searched" for other local minima by rotating the pyridine rings of the bridging ligands relative to one another for both puckered and planar configurations. It is interesting to note that all variations of the planar conformation minimized to a puckered conformation upon completion of the geometry optimization. In addition to the experimentally observed conformational isomers, two other puckered conformers were found, but both were much higher in energy due to a significant "bowing" of the bridging 4,4′-bpy ligands. Since there is no experimental evidence for their existence, the higher energy puckered conformations are not depicted in Figure 1.

Also reported are the results of HF-SCF and DFT-SCF studies for the determination of the molecular wave function and the molecular orbital diagram for the bent conformation of $Re_4(CO)_{12}(4,4'\text{-bpy})_4Cl_4$ (the lowest energy conformation found in the present study). Shown in Figure 7 is a summary of the results from a DFT study utilizing the hybrid functional B3LYP and a 3-21G basis set on the ligand atoms with the SDD basis on the Re metal centers. Similar results were found using different basis functions (LANL2DZ on the Re metals and a STO-3G basis for the ligand atoms) as well as a Hartree−Fock study utilizing a 3-21G basis on the ligand atoms and basis functions with different ECPs on the metals (LANL2DZ or SDD). In all cases the relative orderings of the four highest occupied LCAO-MOs and the four lowest unoccupied LCAO-MOs are the same as those depicted in Figure 7.

At the simplest conceptual level the lowest electronic excitation can be thought of as a promotion of one electron from an occupied MO (normally the HOMO) to an unoccupied MO (normally the LUMO). Therefore, by inspection of the MO diagram, one can describe, in the simplest possible terms, the lowest excited singlet and manifold of triplet states of any molecular system. In the present case the lowest occupied symmetry-adapted MOs (the HOMO is B under the C_2 point group) are composed of $5d_{Re}$ orbitals that are π bonded to the π^*_{CO} orbitals on the CO ligands (called π^*_{CO} back-bonding) and π antibonded with the $2p_{Cl}$ orbitals on the Cl^- ligands. Moreover, the set of lowest

(39) Golub, G. H.; Reinsch, C. *Numer. Math.* **1970**, *14*, 403−420.
(40) Nagle, J. F.; Parodi, L. A.; Lozier, R. H. *Biophys. Soc.* **1982**, *38*, 161−174.
(41) Hofrichter, J.; Henry, E. R.; Sommer, J. H.; Deutch, R.; Ikeda-Saito, M.; Yonetani, T.; Eaton, W. *Biochemistry* **1985**, *24*, 2667−2679.
(42) Hug, S. J.; Lewis, J. W.; Einterz, C. M.; Thorgeirsson, T. E.; Kliger, D. S. *Biochemistry* **1990**, *29*, 1475−1485.
(43) Demas, J. N.; Crosby, G. A. *J. Am. Chem. Soc.* **1970**, *92*, 7262−7270.

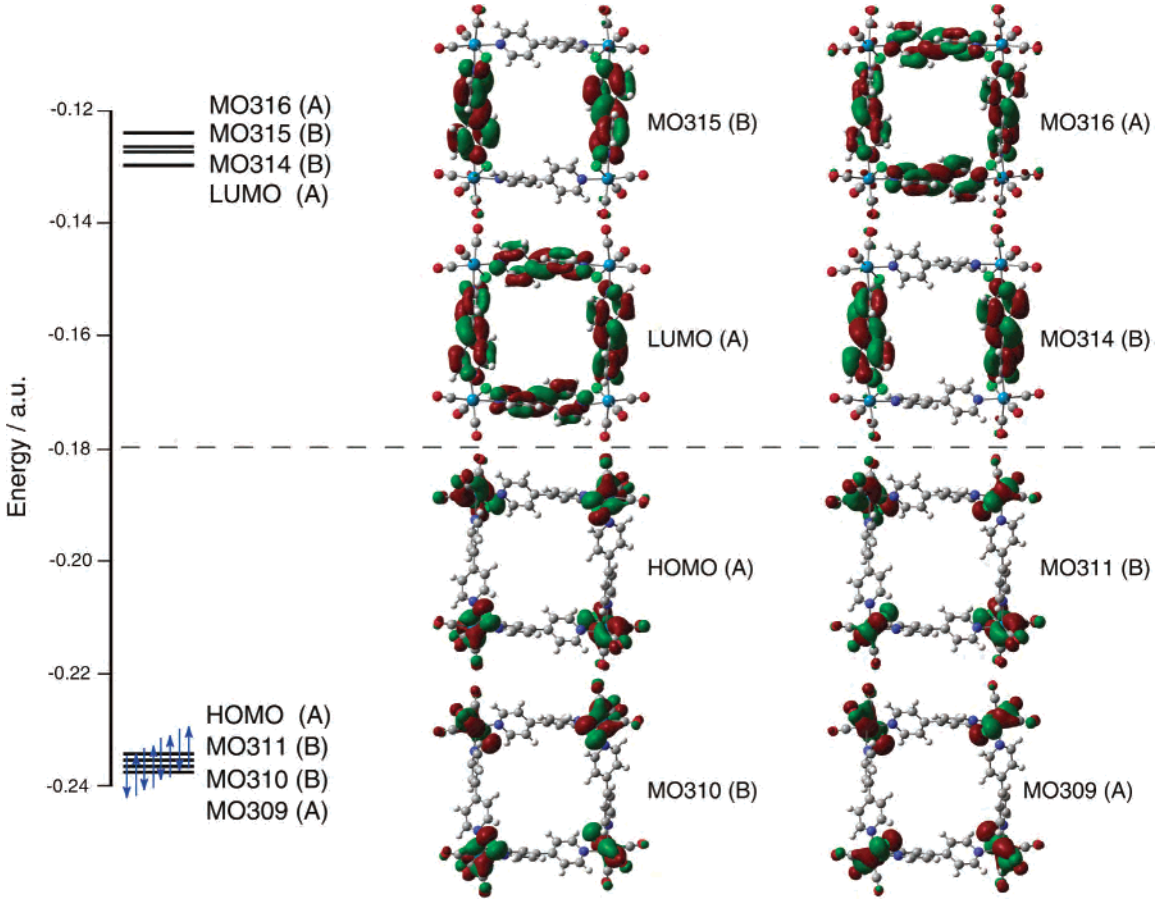

Figure 7. Molecular orbital diagram constructed from a geometry-optimized DFT calculation utilizing the B3LYP functional, 3-21G split basis for ligand atoms, and SDD on the Re centers. The letters in parentheses are symmetry labels based on the C_2 point group. The highest occupied orbitals, including eight more not shown, are primarily $5d_{Re}$ in character, while the lowest unoccupied molecular orbitals are all spatially distributed over the bipyridine ligands.

unoccupied symmetry-adapted MOs (the LUMO is B under the C_2 point group) is composed of all $\pi^*_{4,4'-bpy}$ orbitals located on the bridging 4,4′-bpy ligands. Hence, the lowest set of excited singlet and triplet states can be assigned to a metal-to-ligand charge transfer, or MLCT (mostly $5d_{Re} \rightarrow \pi^*_{4,4'-bpy}$). This is in accordance with the assignments made by other researchers based on spectral evidence alone.[23,30]

Of particular interest is the fact that in the ground-state wave function there is a significant amount of overlap (bonding) between the $5d_{Re}$ orbitals and the π^*_{CO} orbitals. This type of π^*_{CO} back-bonding has been successfully used by a number of researchers as a spectroscopic tag for TRIR experiments involving electronic excitation of transition-metal complexes.[21,22,24,38,44−48] Because electron density on the $5d_{Re}$ orbitals is donated into the π^*_{CO} orbitals, ν(CO) frequency shifts are indicative of changes to the electron density on the Re metals. For example, if a charge transfer takes electron density out of the $5d_{Re}$ orbital upon absorption of a photon, such as a ^{1}MLCT or ^{3}MLCT, then there will be less antibonding character on the CO ligands, resulting in a shift of the ν(CO) frequencies to higher energies (stronger CO bond). Conversely, if an electronic transition transfers more electron density to the $5d_{Re}$ orbitals, then there will be an increase in π^*_{CO} back-bonding and a greater amount of π^* character on the CO ligands, leading to a concomitant shift in the ν(CO) frequencies to lower energies (weaker CO bond). In this way one can track the direction and relative magnitude of charge transfer in this class of multimetallic coordination compounds.

IV. Discussion

(A) Conformers. As described above, after the recrystallization step, the compound was characterized by X-ray diffraction, and the lattice was found to match that reported by Hupp et al., who showed that the pure structural isomer with staggered positioning of the chloride ligands is not exactly square planar.[13] Instead, the rhenium centers lie on the vertices of a tetrahedron. The question remains, however, whether the puckered conformation persists when the crystals are dissolved in acetone. The luminescence data lend some evidence that the rhenium square compound is dispersed in PMMA as a single conformer. It displays a single, broad, and structureless emission band (no shoulders or apparent overlapping bands). Moreover, the lifetime data follow a fit to a single-exponential decay, indicating emission from a

(44) Schoonover, J. R.; Strouse, G. F. *Chem. Rev.* **1998**, *98*, 1335−1355.
(45) Dattelbaum, D. M.; Meyer, T. J. *J. Phys. Chem. A* **2002**, *106*, 4519−4524.
(46) Schoonover, J. R.; Strouse, G. F.; Omberg, K. M.; Dyer, R. B. *Comments Inorg. Chem.* **1996**, *18*, 165−188.
(47) Clark, I. P.; George, M. W.; Johnson, F. P. A.; Turner, J. J. *Chem. Commun.* **1996**, 1587−1588.
(48) Johnson, F. P. A.; George, M. W.; Morrison, S. L.; Turner, J. J. *J. Chem. Soc., Chem. Commun.* **1995**, 391−393.

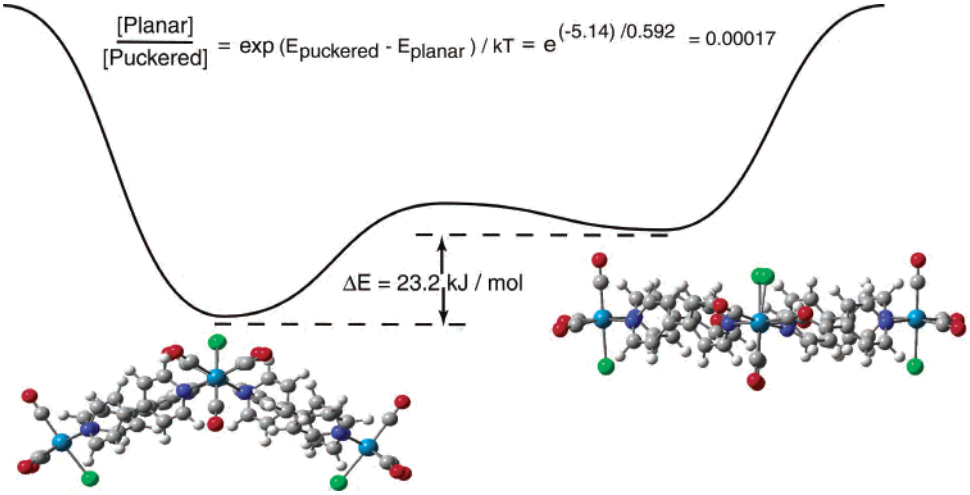

Figure 8. Energy separation between conformers and relative distributions of the different conformers at room temperature. The relative energy difference between conformers was estimated from two separate HF/STO-3G/SDD geometry optimizations.

single thermally equilibrated manifold of states (vide infra). Since the phosphorescence quantum yields could be different for different isomers, it should be noted that the photophysical properties alone do not give definitive evidence of a single conformational isomer present in the sample. Therefore, a combination of spectroscopic (luminescence and TRIR) and theoretical approaches has been used to address this issue in more detail.

To theoretically model the relative energy separation between different conformational isomers, a good deal of effort was put into finding different energy minima during the geometry optimizations of the quantum chemical studies. Starting from various geometries, the calculations converged to four different minima, with the planar conformer being the second lowest in energy, 23.2 kJ/mol above the puckered conformer. Assuming that the acetone does not significantly change this energy difference, if the compound were in thermodynamic equilibrium at room temperature, the planar conformer would be present in ~0.01% of the solute. A schematic diagram of this energy difference is shown in Figure 8. The two other minima would be in even smaller proportions. Therefore, we conclude that the conformer studied in the PMMA films is the puckered one.

A closer consideration of monometallic Re complexes with similar ligands reveals that the puckering of the tetramer is a natural consequence of distortions of octahedral coordination about the rhenium. A planar square would be found if the branching ligands made an angle of greater than or equal to 90°; otherwise, it would relax by forming a tetrahedron. The coordination of the isolated corner has already been studied by Bélanger et al., who performed X-ray diffraction of the monometallic *fac*-tricarbonylchlorobis(4,4′-bpy-*n*)-rhenium.[49] They found the angle formed by the rhenium and the two nitrogen atoms of the bipyridine ligands to be 87°. To remain in a planar conformation would require strain in the bridging ligands, which can be relieved entirely by puckering. The mechanism for stabilizing the planar conformer by disordering the chloride ligands is not as clear. The positioning of the chloride must constrain the direction in which the corner can move, allowing puckering only when the chlorides are staggered.

(B) Orbital Nature of Lowest Triplets. Luminescence data of $Re_4(CO)_{12}(4,4'\text{-bpy})_4Cl_4$ at 77 K in PMMA plastics have revealed a broad structureless emission band and a luminescence lifetime of 18.8 μs. These results are reminiscent of the luminescence properties of related monometallic Re(I) complexes. The most notable is $Re(CO)_3(2,2'\text{-bpy})Cl$, which also displays a broad luminescence band and a microsecond lifetime (3.4 μs at 77 K in PMMA).[50] On the basis of solvent studies, zero-field splitting measurements, TRIR experiments in fluid solution, and quantum chemical modeling, it has been concluded that the luminescence properties of this monometallic complex arise from a spin-forbidden ^{3}MLCT $\rightarrow$ ^{1}GS transition.[35] Likewise, the luminescence properties of $Re_4(CO)_{12}(4,4'\text{-bpy})_4Cl_4$ are also consistent with a spin−orbit perturbed transition from a Boltzmann-populated manifold of ^{3}MLCT states back to the ^{1}GS. Apart from pure spectral evidence, the current study has relied upon a quantum chemical analysis to give insight into the orbital nature of the lowest emitting manifold of triplet states.

It has been shown in many monometallic Re(I) complexes possessing substituted diimine ligands that there are often low-lying ligand-localized excited states ($^3\pi\pi^*$) in close proximity to the ^{3}MLCT excited states and that a change in medium (different solvent polarity or rigid matrixes vs nonrigid matrixes) can alter the ordering between these states.[51] Also, it has been shown that mixing between excited states can affect the excited-state ν(CO) frequencies and account for the infrared "rigidochromism" effect when switching from solution to a 77 K glass or rigid room-temperature PMMA plastic.[45,47] Careful inspection of the

(49) Belanger, S.; Hupp, J. T.; Stern, C. L. *Acta Crystallogr.* **1998**, *C54*, 1596−1600.

(50) Striplin, D. R. In *Chemistry*; Washington State University: Pullman, WA, 1994; p 257.

(51) Sacksteder, L.; Zipp, A. P.; Brown, E. A.; Streich, J.; Demas, J. N. *Inorg. Chem.* **1990**, *29*, 4335−4340.

Table 2. Excited-State Vibrational Frequencies (cm^{-1})[a]

molecule	$A'(1)_{ox}$	$A'(2)_{ox}$	A''_{ox}	$A'(1)_{red}$	$A'(2)_{red}$	A''_{red}	ref
$Re_4(CO)_{12}(4,4\text{-bpy})_4Cl_4$	+22	+56	+64	−17	−7	−6	
$[(dmb)(CO)_3Re(4,4\text{-bpy})Re(CO)_3(dmb)]^{2+}$	+39	+102	+60	−12	−11	−11	20
$(bpy)Re(CO)_3(4\text{-Etpy})$	+20	+68	+20				45
$(bpy)Re(CO)_3Cl$	+20	+58	+36				47

[a] All experiments referenced were conducted in rigid media except for that in ref 20.

ground-state wave function for $Re_4(CO)_{12}(4,4'\text{-bpy})_4Cl_4$ has revealed that the highest 12 occupied MOs are all primarily $5d_{Re}$ in nature. Moreover, the lowest 16 unoccupied MOs are all $\pi^*_{4,4'-bpy}$ in nature, with the closest non-$\pi^*_{4,4'-bpy}$ MO being π^*_{CO} in nature. Therefore, by inspection of the relative ordering of the MOs, one can get an idea of the relative energy gaps between the lowest emitting ^{3}MLCT ($5d_{Re} \rightarrow \pi^*_{4,4'-bpy}$) excited-state manifold and the closest lying $^3\pi\pi^*$ ($\pi_{4,4'-bpy} \rightarrow \pi^*_{4,4'-bpy}$) and ^{3}MLCT ($5d_{Re} \rightarrow \pi^*_{CO}$) excited-state manifolds, which are higher in energy by ~20000 and ~18000 cm^{-1}, respectively. Even though these estimates are derived from a very simplistic point of view, the MO diagram does suggest that the lowest ^{3}MLCT ($5d_{Re} \rightarrow \pi^*_{4,4'-bpy}$) manifold is well separated from the higher $^3\pi\pi^*$ ($\pi_{4,4'-bpy} \rightarrow \pi^*_{4,4'-bpy}$) and ^{3}MLCT ($5d_{Re} \rightarrow \pi^*_{CO}$) manifolds.

(C) Localization and Charge-Transfer Properties. The transient infrared signature indicates a localized charge transfer that has been seen in related bimetallic Re compounds with bipyridine bridging ligands.[20] This is shown by the transient frequency shifts of the carbonyl stretches, which are sensitive to changes in the oxidation state of the rhenium through overlap of the π^*_{CO} and $5d_{Re}$ orbitals, so-called back-bonding.[46] Oxidation of the rhenium, relative to the ground state, pulls electron density out of the π^*_{CO} antibonding state, strengthening the C−O bond, which is manifest by a shift to higher frequency. Reduction has the contrary effect.

Comparing the excited-state spectrum to the ground-state spectrum in Figure 3, one can see that there is no simple shift to higher or lower frequencies: the ground-state peak at 2025 cm^{-1} has shifted to both higher and lower frequencies in the excited state, while ground-state peaks at 1925 and 1890 cm^{-1} are shifted to lower frequencies in the excited state. In all, the excited spectrum is composed of six peaks. Four of these peaks are distinct, while the last two are too small to be resolved. Figure 9 shows a fit to the data with all six components. Thus, the excited state has a reduced metal center in addition to the oxidized center of the ^{3}MLCT.

The transient state must be localized because by inspection of the delocalized states in Figure 7, the oxidation would be spread evenly among all the metals. Then the excited state should have a simple shift of the peaks as seen for monometallic compounds.[47] Instead, the transition must be as shown by the model in Figure 10. In this case the ^{3}MLCT is confined to a single metal center with charge transferred to a neighboring bridging ligand. A small portion of the charge spills over into the bridged metal center, reducing it slightly. This was the model used by Meyer et al. to explain their TRIR data for a bimetallic rhenium compound with bridging bipyridine ligands.[20]

Table 2 compiles the carbonyl frequency shifts for the rhenium square, and includes, for comparison, TRIR data

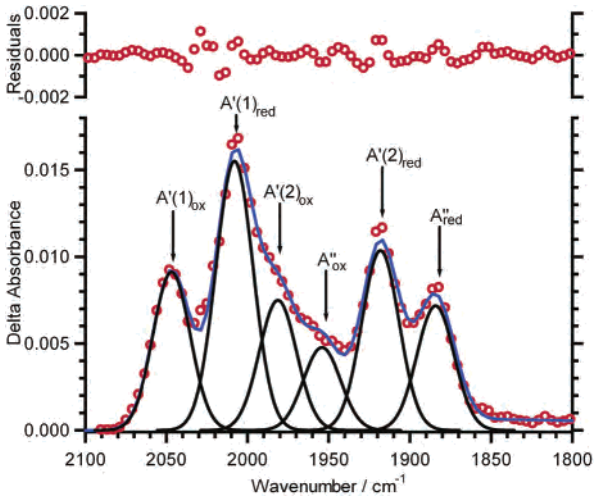

Figure 9. Gaussian fit of the excited-state IR spectrum of $Re_4(CO)_{12}(4,4'\text{-bpy})_4Cl_4$. The symmetry labels are the same as indicated in Figure 4. The subscript "ox" refers to an oxidized Re center, and "red" refers to a reduced Re center.

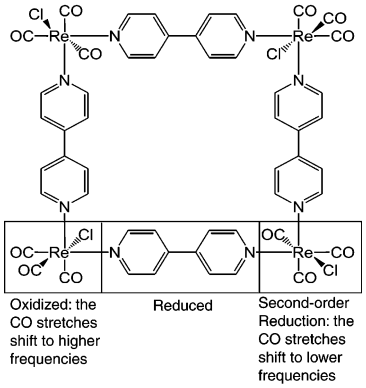

Figure 10. First-order charge transfer from one of the Re metal centers to an adjacent 4,4′-bpy ligand will cause the CO stretches to be shifted to higher frequencies due to a decrease in π^*_{CO} back-bonding. Increased electron density from the transiently reduced 4,4′-bpy can then be donated into the second Re metal, which is attached, causing an increase in π^*_{CO} back-bonding, and the CO stretches will be shifted to lower frequencies.

for monometallic as well as bimetallic compounds. Through a comparison of these transient IR shifts, one can gain some insight into the extent of charge transfer and consequently the extent of localization around each metal center in the Re square complex. It should be noted that there is a marked infrared rigidochromism in the TRIR data of $[Re^I(2,2'\text{-bpy})(CO)_3X]$ complexes (where X = Cl or 4-ethylpyridine) in low-temperature glasses and room-temperature PMMA plastics due to an increased mixing between the lowest ^{3}MLCT ($5d_{Re} \rightarrow \pi^*_{bpy}$) manifold and a higher lying ^{3}MLCT ($5d_{Re} \rightarrow \pi^*_{CO}$) manifold of different orbital parentage.[45,47] Therefore, it is important, for the purpose of comparison, that the TRIR experiments of the $[Re^I(2,2'\text{-bpy})(CO)_3X]$ complexes

be conducted under experimental conditions similar to those of the current study.

Quick inspection of Table 2 shows that the shifts associated with the oxidized Re center in the Re square complex are comparable to the shifts observed for the monometallic complexes, which are good estimates of how much the TRIR peaks will shift in the limit of complete localization. [Note: the TRIR experiments for the Re bimetallic complex was conducted in fluid solution.[20]] Moreover, the second-order reduction observed for the tetrametallic square complex is very similar to that observed for the Re bimetallic complex in which it is known that the ^{3}MLCT is localized between the bridging bipyridine and a single Re metal. Therefore, one can conclude that the charge transfer ($5d_{Re} \rightarrow \pi^*_{bpy}$) in $Re_4(CO)_{12}(4,4'\text{-bpy})_4Cl_4$ is highly localized between a single Re metal and bridging ligand and the transient mixed-valence state is strictly localized.

V. Conclusions

The electronic symmetry of the excited states of many transition-metal complexes has been hotly debated for a number of years. This issue is just as important for multimetallic transition-metal complexes but has the added twist that transient mixed valency between metal centers can dramatically augment the photophysical properties in such compounds. The present study has addressed the spectroscopic properties of $Re_4(CO)_{12}(4,4'\text{-bpy})_4Cl_4$, has attempted to give greater insight into the orbital nature of the lowest emitting triplet manifold, and has modeled the relative energies and populations of the lowest ground-state conformational isomers. The major conclusions are as follows. The lowest energy conformer is that of the puckered geometry, and the energy difference between the puckered and planar geometry is such that the planar geometry is present in less than 0.01% under the present experimental conditions. The orbital assignment of the lowest emitting triplet manifold originates from a $\pi^*_{4,4'-bpy} \rightarrow 5d_{Re}$ electronic transition and is fully corroborated by a quantum chemical modeling study. In conjunction with the state assignment for the lowest triplet manifold, all spectroscopic evidence leads to the conclusion that this lowest ^{3}MLCT is localized between a single Re metal center and an adjacent bridging ligand. Moreover, TRIR studies on $Re_4(CO)_{12}(4,4'\text{-bpy})_4Cl_4$ and a comparison with the TRIR behavior of related monometallic Re(I) complexes clearly show that the transient mixed valency is strictly localized in the excited state, which increases the oxidation state of a single Re metal from +1 to +2. Finally, it has been observed that there is a second-order charge transfer between the transiently reduced bridging ligand and the nonoxidized Re center to which it is attached, effectively lowering its oxidation state.

Acknowledgment. We acknowledge a grant from Sandia National Laboratories, SURP program, for support of this research. The University of New Mexico is also thanked for financial and programmatic support.

IC034560L